TS-1 from First Principles[†]

Aldo Gamba,* Gloria Tabacchi, and Ettore Fois

Dipartimento di Scienze Chimiche ed Ambientali, University of Insubria, and INSTM, Via Lucini 3, I-22100 Como, Italy

Received: May 31, 2009; Revised Manuscript Received: July 22, 2009

First principles studies on periodic TS-1 models at Ti content corresponding to 1.35% and 2.7% in weight of TiO_2 are presented. The problem of Ti preferential siting is addressed by using realistic models corresponding to the TS-1 unit cell [$TiSi_{95}O_{192}$] and adopting for the first time a periodic DFT approach, thus providing an energy scale for Ti in the different crystallographic sites in nondefective TS-1. The structure with Ti in site T3 is the most stable, followed by T4 (+0.3 kcal/mol); the less stable structure, corresponding to Ti in T1, is 5.6 kcal/mol higher in energy. The work has been extended to investigate models with two Ti's per unit cell [$Ti_2Si_{94}O_{192}$] (2.7%). The possible existence of Ti−O−Ti bridges, formed by two corner-sharing TiO_4 tetrahedra, is discussed. By using cluster models cut from the optimized periodic DFT structures, both vibrational (DFT) and electronic excitation spectra (TDDFT) have been calculated and favorably compared with the experimental data available on TS-1. Interesting features emerged from excitation spectra: (i) Isolated tetrahedral Ti sites show a Beer−Lambert behavior, with absorption intensity proportional to concentration. Such a behavior is gradually lost when two Ti's occupy sites close to each other. (ii) The UV−vis absorption in the 200−250 nm region can be associated with transitions from occupied states delocalized on the framework oxygens to empty d states localized on Ti. Such extended-states-to-local-states transitions may help the interpretation of the photovoltaic activity recently detected in Ti zeolites.

1. Introduction

TS-1, titanium silicalite, is a porous, crystalline material broadly used in industrial plants as a catalyst for hydrocarbon oxidative processes.[1] Since it allows operation at mild conditions using hydrogen peroxide as the oxygen source and generating water as a byproduct, its discovery[2] is considered a milestone in the development of modern heterogeneous catalysts for sustainable technologies. For this reason, TS-1 has been one of the most extensively studied zeolitic materials, and much attention is still focused on its unique physicochemical and reactivity properties. In addition to its relevance in catalysis, TS-1 is currently of interest for advanced applications in other fields, such as solar cell technology. Indeed, titanium zeolites have recently been shown to exhibit photovoltaic activity,[3] thus suggesting their use in dye-sensitized solar cells as porous electron-transport materials as an alternative to dense TiO_2 nanoparticles.

From a structural point of view, TS-1 is a zeolite with a MFI framework topology.[4] The all-silica phase of MFI, the catalytically inactive Silicalite-1, has a unit cell content corresponding to [$Si_{96}O_{192}$]. The as-synthesized Silicalite-1, containing tetrapropylammonium cation as the structure directing agent (SDA), has an orthorhombic structure.[5] The calcined form of Silicalite-1 has a monoclinic unit cell with $\alpha = 90.6°$.[6] The catalytically active phase TS-1, which is characterized by a low Ti content (below 3.0% in weight of TiO_2), is orthorhombic.[6] It can be considered a solid solution of TiO_2 in zeolitic SiO_2, in which only a small portion of the tetrahedral sites (T sites) are isomorphously occupied by Ti. Thus, in TS-1 and, in general, in titanium zeolites, Ti is surrounded by four oxygen atoms in a tetrahedral environment and is therefore undercoordinated with respect to the stable TiO_2 phases, in which Ti occupies octahedral sites (TiO_6). Indeed, it is believed that such a Ti fourfold coordination is actually responsible for the Ti zeolites' catalytic activity, because TiO_2 contents higher than 3% lead to phase separation of octahedral TiO_2 phases and deactivation of the catalytic properties of the material.[7]

In view of its role in industrial catalysis, TS-1 has been the subject of many experimental investigations carried out with a variety of spectroscopic techniques. Despite the broad benchmark of UV−vis, IR, Raman, and X-ray data on Ti sites in TS-1 available in the literature,[8−11] details of the TS-1 structure at the microscopic level are still unclear. One such issue is concerned with the Ti location in TS-1. Diffraction studies[12−14] have suggested a nonrandom distribution of Ti in the tetrahedral T sites of TS-1. However, there is still no general consensus on the T sites actually occupied by Ti in TS-1, and different siting probabilities were reported.[15]

The uncertainty in locating Ti is associated with the low Ti concentration, corresponding to approximately 2−3 Ti atoms in the TS-1 unit cell. Moreover, due to its large unit cell size and low Ti content ([$Ti_xSi_{96-x}O_{192}$]), to date, this crystalline catalyst has escaped a thorough theoretical characterization. Studies aimed at establishing the location of the Ti in TS-1 have been performed only by adopting force-field-based schemes[16,17] or quantum mechanical methods on cluster or embedded cluster models.[15,18]

The primary goal of this work is to fill this gap by performing a series of density functional theory (DFT) calculations by using for the first time a first-principles periodic approach for such a large system.

Although the high calcination temperature needed to obtain the active TS-1 catalyst may suggest a role of thermodynamics in establishing the Ti distribution in the different T sites, the microscopic origin of Ti preferential siting is still a matter of

[†] Part of the "Vincenzo Aquilanti Festschrift".

* Corresponding author. E-mail: Aldo.Gamba@uninsubria.it.

10.1021/jp905110s
Published on Web 09/28/2009

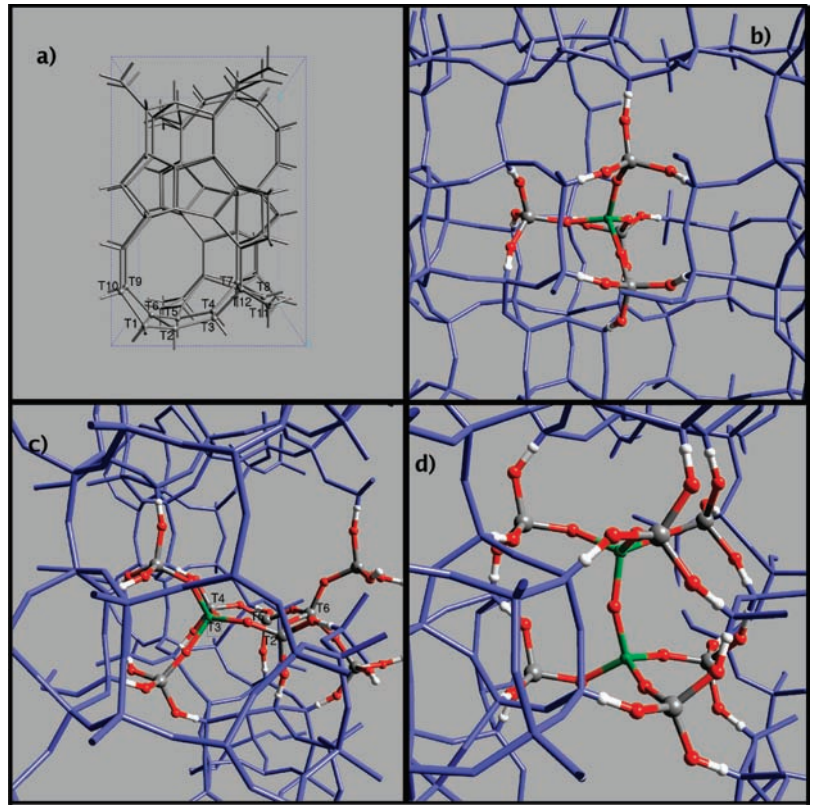

Figure 1. (a) Graphical representation of the MFI unit cell. Only T atoms are represented. Also reported are the labels of the 12 independent T sites. (b) Ball-and-stick Ti[O-(Si(OH)$_3$]$_4$ cluster (C_{tetra}) superimposed on the TS-1 crystal (blue sticks). Color codes: Si, gray spheres; O, red spheres; H, white spheres; Ti, green sphere. (c) Ball-and-stick representation of a $C_{5\text{-ring}}$ cluster superimposed on the TS-1 crystal (blue sticks). Color codes: Si, gray spheres; O, red spheres; H, white spheres; Ti, green sphere. (d) Ball-and-stick representation of a Ti−O−Ti bridge structure (C_{2tetra} cluster) superimposed on the TS-1 crystal (blue sticks). Color codes: Si, gray spheres; O, red spheres; H, white spheres; Ti, green spheres.

discussion, and a series of hypotheses have been formulated.[12,15,19] It has been proposed that kinetic factors may be the predominant ones in determining the actual Ti location.[15] In addition, it has been suggested that, already during the nucleation and growth process, Ti siting may be influenced by the distribution of the structure directing agent because of the coulomb interactions between positively charged SDAs and pentavalent anionic (hydroxylated) Ti centers detected in as-synthesized (noncalcined) TS-1.[19] Moreover, it has been reported that the disappearance of defect centers (e.g., Si−OH groups) correlates with an increase in Ti concentration, suggesting the idea that Ti replaces defective sites in TS-1.[12] In this scenario, our work is aimed at establishing an energy scale for Ti occupancy in the different tetrahedral sites of TS-1 by using a periodic DFT approach.

Since in the orthorhombic MFI framework there are 12 crystallographically different tetrahedral sites, geometry optimizations have been carried out on 12 [$TiSi_{95}O_{192}$] structures obtained by placing Ti in one of the 12 inequivalent T positions. These structures correspond to a title of 1.35% in weight of TiO_2. Optimizations have been also performed on structures characterized by a [$Ti_2Si_{94}O_{192}$] stoichiometry to explore the energetics of TS-1 models at a 2.7% Ti content. In this case, a systematic computational investigation is prevented by the number of possible structures: because there are 12 T sites, each with multiplicity 8, there are $96!/(2!(96-2)!) = 4608$ possible structures characterized by different location of 2 Ti atoms. However, relevant insight has been gathered by focusing the analysis on a restricted subset of models, thus enabling quantification of the energy separation among the different Ti distributions for a TS-1 framework characterized by a Ti content close to that typical of the actual catalytic material.

In addition to energetic issues related to Ti siting, electronic and vibrational properties of Ti in the different tetrahedral sites of the TS-1 model systems were studied. A thorough analysis has been performed on electronic excitation spectra in the UV−vis region, where a signature of zeolitic titanium is detected at around 200−250 nm.[20] Moreover, IR and Raman spectra were calculated and compared with the corresponding spectroscopic data,[8,9] which also exhibit fingerprints of framework Ti. From such a theoretical characterization of Ti sites, combined with the analysis of their energy stability, reliable predictions about the Ti distribution in TS-1 could be deduced.

2. Methods of Calculations and Models

The orthorhombic framework of TS-1 (space group *Pmna*; see, e.g., ref 12) is characterized by interconnected channels whose section is formed by 10-membered rings. The secondary building unit is a 5−1 structure characterized by a 5-membered ring (5-ring).[4] There are 12 nonequivalent T sites (each with multiplicity 8) and 26 nonequivalent O sites (see Figure 1). The 12 possible structures [$TiSi_{95}O_{192}$], identifiable by the location of Ti in one of the 12 sites (labeled T1, T2, T3, ..., T12), were studied by adopting plane waves as the basis set and the PBE gradient-corrected DFT functional.[21] The geometry of each of the 12 [$TiSi_{95}O_{192}$] systems (T1, T2, ..., T12 from now on) was optimized by using ultrasoft Vanderbilt pseudopotentials[22] with a 30 Ry cutoff for the plane wave expansion of the orbitals and a 180 Ry cutoff for the electronic density (PBE/VDB/30) at the Γ point. Periodic boundary conditions were applied.

Such a computational scheme, based on ultrasoft pseudopotentials and PBE approximation to DFT, has been successfully adopted in the study of the structure and the energetics of large

systems, such as TiO_2 surfaces[23] and aluminosilicate porous materials.[24] Moreover, the PBE approximation has proven reliable for the structure and energetics of other heteroatom-substituted zeolite structures, such as boron zeolites.[25,26]

Optimizations were carried out using a quasi-Newton scheme, at fixed cell parameters (fixed volume), but no constraint was imposed on the nuclear positions. Optimizations were considered converged when the maximum force on the atoms was less than 10^{-4} a.u. The CPMD code[27] was used for the plane wave periodic DFT calculations. The cell parameters adopted in the calculations ($a = 20.049$ Å, $b = 19.926$ Å, $c = 13.401$ Å), are extracted from diffraction studies on TS-1 with corresponding Ti content.[12] With the same computational setup, we have optimized the structures of a few $[Ti_2Si_{94}O_{192}]$ models, obtained by placing Ti in two T sites and adopting cell parameters ($a = 20.113$ Å, $b = 19.930$ Å, and $c = 13.410$ Å) corresponding to a TS-1 sample of comparable Ti content.[12]

For the electronic excitation spectra calculations, two different approaches were adopted. In one, the cluster approach, time-dependent DFT (TD-DFT)[28,29] calculations were carried out on Ti-containing clusters cut from the PBE/VDB/30-optimized periodic structures. Three cluster models of different sizes were adopted; namely, C_{tetra}, $C_{5\text{-ring}}$, and C_{2tetra}, represented in Figure 1. In the smallest model, C_{tetra}, with stoichiometry $Ti-[O-(Si(OH)_3]_4$, Ti is surrounded by four tetrahedral building units, that is, by two oxygen atoms shells. Oxygens in the second shell were saturated with H atoms located at 1.0 Å from O, along the O−Si bond direction in the corresponding optimized crystal structure. Cluster $C_{5\text{-ring}}$ contains a 5-ring structure and is characterized by a $Ti_xSi_{9-x}O_9(OH)_{18}$ stoichiometry, whereas C_{2tetra} is formed by two corner-sharing C_{tetra} clusters and has a $Ti_xSi_{8-x}O_7(OH)_{18}$ formula. Systems with $x = 0, 1, 2$ have been considered. The $C_{5\text{-ring}}$ and the C_{2tetra} clusters were used, with $x = 2$, to investigate the properties of Ti−O−Si−O−Ti and Ti−O−Ti bridges, respectively. The external oxygen atoms were saturated by the same procedure adopted in the C_{tetra} model. TD-DFT excitations were calculated using the hybrid B3LYP functional[30] and a Gaussian basis set (6-311+g**).[31] Convergence was required for at least 50 excited states. We shall refer to these results as TDDFT/cluster.

In a second approach, the electronic excitation spectrum was calculated by adopting periodic boundary conditions. Specifically, the optical conductivity of the PBE/VDB/30 optimized structures was calculated by using the PBE functional and norm-conserving pseudopotentials[32,33] with a cutoff of 110 Ry for the plane wave expansion of the orbitals and 440 Ry for the electronic density. In the case of large periodic systems, the more accurate TD-DFT approach for electronic excitations is not viable; however, gradient-corrected DFT gives results quite close to TD-DFT in the case of Ti−zeolite systems.[34−36] We shall refer to these calculations as DFT/pbc. In the calculated electronic excitation spectra, both DFT/pbc and TDDFT/cluster, a line broadening of 2.0 nm was applied.

Vibrational properties, IR and Raman, were calculated on the above-described cluster models. To this aim, the cluster geometries have been reoptimized using the B3LYP functional and the 6-311+g** basis set. In the minimization process, the "external" O−H atoms were kept fixed to mimic the constraint due to the full crystal and to decouple the calculated vibrational spectra from signals due to modes involving O−H groups. Such modes are known to interfere in the silica window, an otherwise transparent region between 850 and 1000 cm^{-1} typical of SiO_2 materials, where signals of tetrahedral Ti can be found. All the spectra are calculated within the harmonic approximation and obtained from stationary points, characterized by positive frequencies. A line-broadening of 10 cm^{-1} was used for both IR and Raman spectra representations. As common practice in comparing with experimental data, a shift factor of 0.98 was applied to the calculated wavenumbers.[37]

TABLE 1: Calculated ΔE (in kcal/mol), Optimized Ti−O Bond Distances and Average <Ti−O> Distances vs T Site[a]

	ΔE	Ti−O	Ti−O	Ti−O	Ti−O	<Ti−O>
T1	5.59	1.7855	1.7928	1.7955	1.7965	1.7926
T2	3.87	1.7912	1.7914	1.7971	1.7984	1.7945
T3	0.0	1.7827	1.7905	1.7931	1.8040	1.7925
T4	0.28	1.7895	1.7965	1.7971	1.7989	1.7955
T5	2.84	1.7935	1.8006	1.8013	1.8030	1.7996
T6	4.92	1.7919	1.7952	1.7959	1.8039	1.7967
T7	4.06	1.7881	1.7936	1.7962	1.8085	1.7966
T8	2.29	1.7778	1.7934	1.7959	1.8105	1.7944
T9	2.23	1.7803	1.7978	1.7987	1.8042	1.7953
T10	4.20	1.7923	1.7951	1.7969	1.8039	1.7971
T11	1.41	1.7929	1.7943	1.8041	1.8096	1.8002
T12	1.48	1.7867	1.7917	1.8023	1.8048	1.7964

[a] Distances in angstroms.

TABLE 2: Optimized O−Ti−O Bond Angles and Average O−Ti−O Bond Angle (<OTiO>) vs T Site[a]

							<OTiO>
T1	108.7	113.3	111.0	107.5	108.6	107.6	109.4
T2	108.2	107.8	110.3	107.5	112.5	110.4	109.4
T3	109.9	108.0	110.5	107.3	109.5	111.6	109.5
T4	110.3	105.6	112.0	108.3	109.7	110.9	109.5
T5	110.5	106.6	108.8	109.9	108.6	112.3	109.5
T6	109.0	109.8	109.4	110.8	106.9	110.9	109.5
T7	108.1	108.5	109.9	108.2	112.2	109.7	109.5
T8	109.0	108.6	106.9	111.5	108.7	112.0	109.4
T9	110.0	109.4	110.1	106.1	110.5	110.6	109.5
T10	109.4	110.3	109.6	108.3	109.7	109.5	109.5
T11	107.4	108.8	110.9	108.6	110.6	110.4	109.5
T12	108.7	109.3	112.0	110.1	109.4	107.2	109.5

[a] Angles in degrees.

3. Results

3.1. Structure and Energetics. The minimum energy structure among the 12 $[TiSi_{95}O_{192}]$ models corresponds to the one where Ti occupies site T3. Such a structure is, however, only 0.28 kcal/mol below the one with Ti in T4, whereas the highest energy structure, 5.6 kcal/mol above the T3, corresponds to Ti in T1. Therefore, it turns out that energy differences among TS-1 systems characterized by 1.35% Ti are within 5.6 kcal/mol. Remarkably, 9 out of 12 structures are within the 4 kcal/mol range from the mimimum.

The calculated Ti−O bond distances and O−Ti−O bond angles are reported in Tables 1 and 2, respectively. It should be said at the outset that all Ti sites have a slightly distorted tetrahedral structure. In general, the calculated Ti−O bond lengths are in agreement with the value of 1.793 Å reported from in vacuo X-ray spectroscopies studies on calcinated TS-1 samples.[11] The trends of (i) average Ti−O bond distances, (ii) Ti−Si (first-neighbors) distances, and (iii) Ti−O−Si angles as a function of Ti siting in the 12 $[TiSi_{95}O_{192}]$ optimized structures are reported in Figure 2 along with the energy differences, ΔE. Also reported in Figure 2 are the (normalized) probabilities associated with Ti occupancy of the different T sites. Probabilities were calculated, from the Boltzmann factor $\exp(-\Delta E/kT)$, for room temperature and for 500 °C, a commonly adopted calcination temperature. It can be deduced, on purely energetics

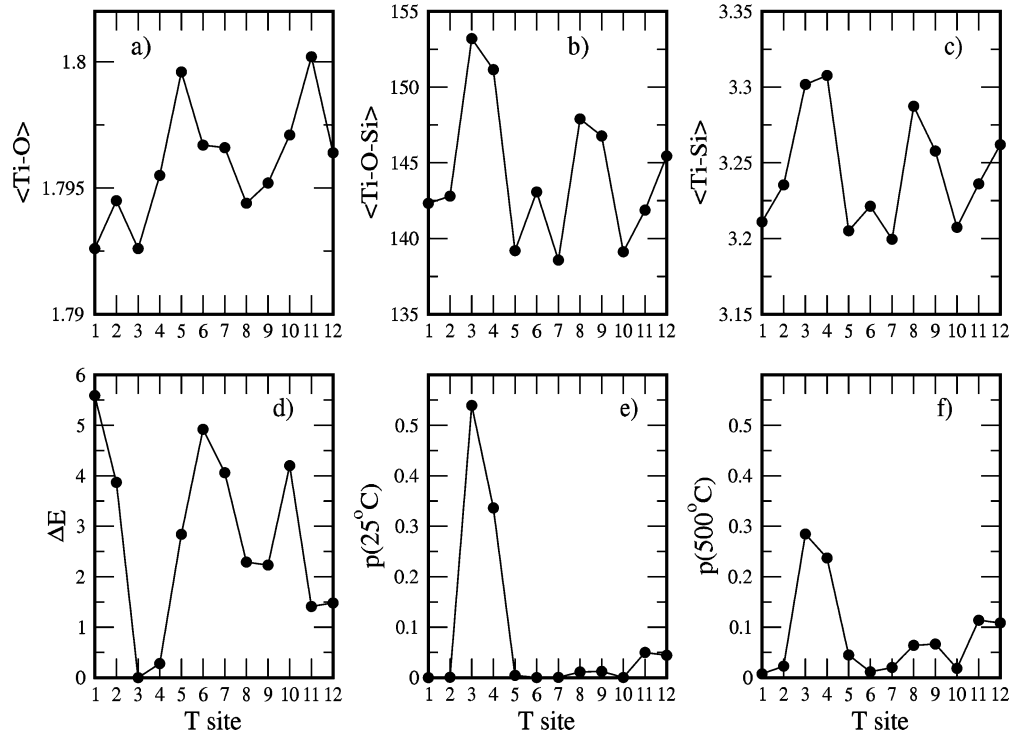

Figure 2. Selected properties of [$TiSi_{95}O_{192}$] characterized by different siting of Ti. (a) Average Ti−O bond distances (in Å) for different Ti sitings. (b) Average Ti−O−Si angles (in degrees) for different Ti sitings. (c) Average Ti−Si separation (in Å) for different Ti sitings. (d) PBE/VDB/30 ΔE (in kcal/mol) calculated with respect to Ti in T3. (e) Normalized probability of occurrence of Ti in the 12 T sites at 25 °C. (f) Normalized probability of occurrence of Ti in the 12 T sites at 500 °C.

grounds, that the T3 and T4 sites would account for more than 50% of Ti, even at high calcination temperatures.

Selected configurations with stoichiometry [$Ti_2Si_{94}O_{192}$], corresponding to two Ti's per unit cell, have been optimized, as well. They represent only a subset of the many possible configurations with such a Ti content. In all cases, one Ti (Ti^1) was placed in one T3 site, corresponding to the minimum energy monosubstituted structure, while the location of the second Ti (Ti^2) varied, and a total of 20 different configurations were optimized. The Ti^1-Ti^2 pairs, their Ti−Ti distances, and the relative stability are graphically represented in Figure 3. The most stable system corresponds to a configuration with Ti^2 in a T4 site at about 7.3 Å from Ti^1. However, most of the optimized structures are within 6 kcal/mol from the minimum energy arrangement. It should be noted that the energy difference depends not only on the pair of sites but also on their actual separation. On the other hand, in the case of Ti in T3−T5, two T5 sites are available at similar distances from T3 (at about 5.2 Å), but the two corresponding arrangements differ by 1.3 kcal/mol. This finding indicates that also the details of the Ti centers' local environments may affect the relative stability of systems characterized by different Ti distributions.

Two systems containing adjacent T sites, characterized by a Ti−O−Ti bridge and a Ti−Ti distance of ∼3.5 Å, were also considered: the first one, and most stable of the two, with the second Ti (Ti^2) in T4 and the second structure with Ti^2 in T6. The two structures differ by 4.3 kcal/mol; therefore, for systems with corner-sharing TO_4, the relative energy depends on the pair of T sites actually occupied by Ti. Remarkably, the T3−T4 Ti−O−Ti bridge structure is only 2.7 kcal/mol higher than the most stable system with the same Ti content. Its Ti−O bond distances and O−Ti−O angles, reported in Tables 3 and 4, respectively, are very close to the ones calculated for the systems containing a single Ti site. This indicates that the formation of a Ti−O−Ti bridge implies only small distortions in the geometry of the TiO_4 units. Moreover, the Ti−O−Ti bonds forming the bridge are the shortest ones among the systems here considered.

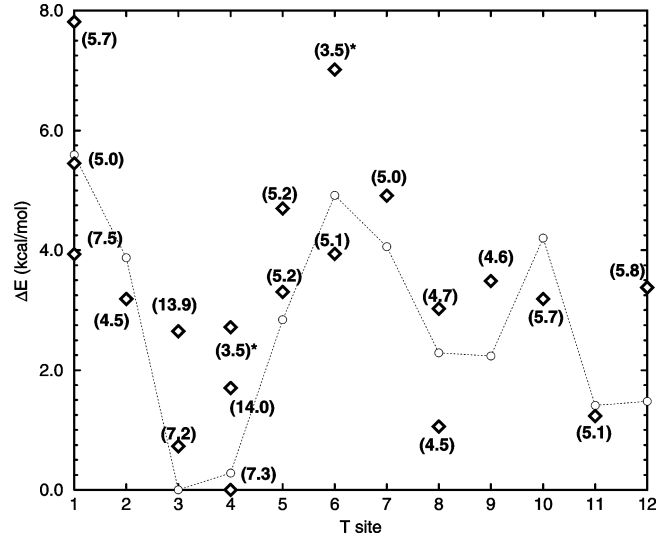

Figure 3. Energy differences, ΔE in kcal/mol, of selected [$Ti_2Si_{94}O_{192}$] configurations. In all configurations, Ti^1 is positioned in T3. They differ by the siting of Ti^2. The diamonds represent the energy relative to the most stable configuration among the sampled ones (Ti^1 in T3 and Ti^2 in T4), with the corresponding Ti^1-Ti^2 distance (in Å) reported in parentheses. Configurations labeled with a star are characterized by a Ti−O−Ti bridge. Circles connected by a dashed line represent the energy scale for a single Ti substitution ([$TiSi_{95}O_{192}$]).

3.2. Vibrational Analysis. IR and Raman spectra have been of overwhelming relevance in unraveling the structure of the Ti sites in TS-1 and related materials.[8,9] An IR feature at 960 cm^{-1} has been associated with Ti in zeolitic tetrahedral sites.

TABLE 3: Optimized Ti−Ti Separation and Ti−O Bond Distances for a [$Ti_2Si_{94}O_{192}$] Structure Characterized by Ti in T3 and T4 with a Ti−O−Ti Bridge[a]

	Ti−Ti	Ti−O*	Ti−O	Ti−O	Ti−O	<Ti−O>
T3	3.4952	1.7761	1.7949	1.7978	1.8016	1.7918
T4	3.4952	1.7870	1.7934	1.7940	1.7976	1.7930

[a] The Ti−O* entry refers to the Ti−O−Ti bonds. Distances in angstroms.

TABLE 4: Optimized O−Ti−O Bond Angles and Average O−Ti−O Bond Angle (<OTiO>) for a [$Ti_2Si_{94}O_{192}$] Structure Characterized by Ti in T3 and T4 with a Ti−O−Ti Bridge[a]

							<OTiO>
T3	106.1	108.1	108.3	109.6	111.8	112.6	109.4
T4	106.2	106.9	108.6	109.1	111.8	114.1	109.5

[a] Angles in degrees.

Moreover, the intensity of such a band has been proved to be related to the content of tetrahedral Ti in TS-1.[38] In addition, a Raman signature at 1125 cm^{-1} has been associated with tetrahedral Ti. In Figure 4a, the calculated IR and Raman predictions are shown for a Ti-containing cluster and for the equivalent all-silica one. The spectrum of the T3-centered C_{tetra} system is reported in Figure 4a, along with that calculated for a $C_{5\text{-ring}}$ with one Ti in T3. Because clusters centered on different crystallographic T sites have very similar vibrational properties, only the T3 case will be discussed. In the small C_{tetra} cluster, a peak at about 980 cm^{-1} (with a shoulder at 1005 cm^{-1}) is associated with the presence of Ti, both in the IR and in the Raman predictions. In the larger $C_{5\text{-ring}}$ system, the 980 cm^{-1} feature is red-shifted to 958 cm^{-1}. In the Raman activity spectrum, the small C_{tetra} cluster shows an intense peak at 1128 cm^{-1}, which is shifted to 1135 cm^{-1} in the $C_{5\text{-ring}}$. In both cases, such a Raman-active mode is related to an in-phase (symmetric) stretching of the TiO_4 unit. It should be pointed out that the above-discussed features are missing in the spectra of an all-silica $C_{5\text{-ring}}$ cluster reported in Figure 4a for comparison and should, therefore, be attributed to the presence of tetrahedral Ti. Remarkably, both IR and Raman results are in line with experimental findings.[8,9]

In Figure 4b and c, the vibrational spectra calculated for clusters containing two close Ti atoms are shown: one is relative a Ti−O−Ti bridge; the other, to a Ti−O−Si−O−Ti structure. Let us discuss the vibrational properties of a C_{2tetra} system containing a Ti−O−Ti bridge (Figure 4b). In the IR spectrum, such a system is characterized by two Ti-related features, at 853 and 1006 cm^{-1}, both located at the edges of the silica window. A very intense Raman-active peak is found at 1114 cm^{-1}; two weaker Raman signals are found at 978 and 1003 cm^{-1}. In addition, a very weak Raman signal is calculated at 853 cm^{-1}. The above IR and Raman signals are due to the Ti−O−Ti bridge because they are missing in the spectra of the other C_{2tetra} clusters, reported in Figure 4b, that do not contain such a bridge.

In the case of a $C_{5\text{-ring}}$ characterized by a Ti−O−Si−O−Ti bridge (Figure 4c), the IR signal at 958 cm^{-1} typical of an isolated tetrahedral Ti is enhanced in intensity; however, a new feature appears at 908 cm^{-1}. In the Raman spectrum, the 1135 cm^{-1} signal typical of isolated Ti is split and red-shifted at 1110 cm^{-1}. The 958 cm^{-1} Raman feature is red-shifted to 908 cm^{-1} in passing from a $C_{5\text{-ring}}$ with only one Ti to a $C_{5\text{-ring}}$ with a Ti−O−Si−O−Ti bridge. The above-discussed features are absent (both IR and Raman) in the all-silica $C_{5\text{-ring}}$ system spectra reported in Figure 4c for comparison.

3.3. Electronic Excitation Spectra. UV−vis spectra of dry TS-1 and other Ti zeolites are characterized by a broad absorption band at 200−250 nm,[9,20,39] which is considered the fingerprint of tetracoordinated Ti in the zeolite framework. Band profiles, as well as maximum position and intensity, slightly vary among the wealth of available experimental data. For instance, a 208−210 nm peak position is reported for dry TS-1,[11,40] but other studies on the same system reported, after deconvolution, a strong peak at 199 nm and two weaker bands at 226 and 248 nm.[10] However, general agreement exists in interpreting these bands as ligand-to-metal charge transfer (LMCT) transitions from occupied oxygen states to empty Ti d orbitals in tetrahedral TiO_4 units.

Combination of periodic DFT calculations with the TDDFT/cluster approach provides a reliable theoretical description of electronic properties of zeolitic Ti.[35] Unless otherwise stated, the results here presented refer to TD-DFT excitations calculated for clusters extracted from optimized PBE/VDB/30 models.

The electronic excitation spectra calculated for the 12 Ti-centered C_{tetra} clusters, reported in Figures 5 and 6, show absorptions in the 200−230 nm region typical of experimental spectra of Ti zeolites. To exclude that calculated excitations are derived from artifacts of the adopted approximations, the electronic spectrum of a T1 cluster extracted from silicalite was calculated, as well. By comparing the Ti- and Si-centered systems (Figure 5), it clearly emerges that the 200−230 nm band is due to tetrahedral TiO_4, in line with the current interpretation and with previous theoretical studies.[35,36] Moreover, calculations for Ti in the T6 site performed on both C_{tetra} and $C_{5\text{-ring}}$ clusters provided analogous electronic structure descriptions and very close wavenumbers for the lowest energy transition ($\Delta\lambda_{max} = 1.1$ nm). Therefore, the results presented below are not significantly affected by cluster size effects.

Calculated electronic excitation spectra show different profiles but are all characterized by multiple peaks. The presence of multiple bands derives, in general, from the splitting of the empty Ti 3d and of the occupied O 2p states as a consequence of the quasi-tetrahedral T-site environment, as highlighted by previous work on different Ti-zeolites.[36] By a thorough analysis of the electronic structure in terms of the molecular orbitals involved in the excitations, a detailed description of the electronic transitions that characterize Ti in the 12 different T sites can be obtained.

In the C_{tetra} (Ti−[O−($Si(OH)_3$]$_4$) clusters, the lower energy empty molecular orbitals (MO) are mostly localized on Ti and may be described in terms of crystal field theory (CFT) in the case of tetrahedral coordination. More specifically, the two lowest empty MOs, the LUMO and LUMO + 1, may be correlated with the Ti d_{z^2} and Ti $d_{x^2-y^2}$ states, whereas the MOs from LUMO + 2 to LUMO + 7 are due to combinations of Ti d_{xy}, d_{xz}, and d_{yz} with framework oxygen lone pairs (Figure 7). By borrowing the familiar CFT notation, we shall refer to these two groups of states as $e_g^{(E)}$ and $t_{2g}^{(E)}$ respectively, where (E) stays for "empty". However, at difference with the case of an ideal tetrahedron, here degeneracy of the $e_g^{(E)}$ and of the $t_{2g}^{(E)}$ states is removed because TS-1 actually provides distorted tetrahedral environments to the metal center. In addition, such distortions are different for each T site and not only depend on the local TiO_4 geometry but also are related to Ti−Si separations, Ti−O−Si angles, and in general, to the arrangement of the SiO_4 units around Ti. This leads to slightly different orbital splitting patterns among the 12 model systems; in particular, $e_g^{(E)}$ and $t_{2g}^{(E)}$ states are separated by energy differences ranging from 0.58

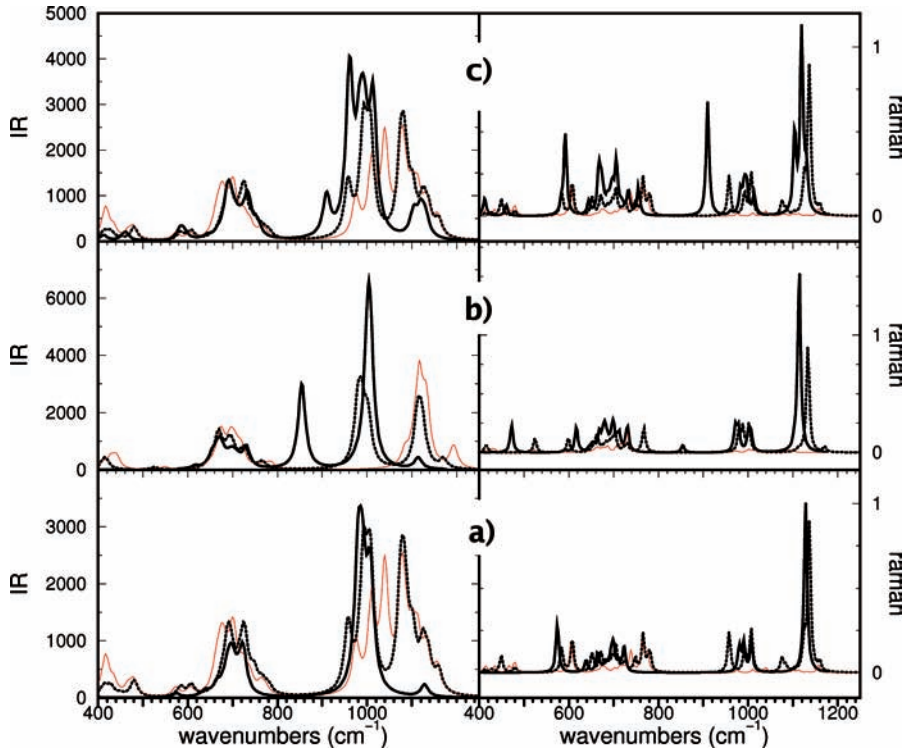

Figure 4. Calculated IR (left panels) and Raman (right panels) intensities. (a) Solid line: C_{tetra} with Ti in T3. Dashed line: $C_{5\text{-ring}}$ with Ti in T3. Red line: all-silica $C_{5\text{-ring}}$. (b) Solid line: C_{2tetra} with a Ti−O−Ti bridge, Ti in T3 and T4. Dashed line: C_{2tetra} with one Ti in T3. Red line: all-silica C_{2tetra}. (c) Solid line: $C_{5\text{-ring}}$ with a Ti−O−Si−O−Ti bridge, Ti in T3 and T6. Dashed line: $C_{5\text{-ring}}$ with one Ti in T6. Red line: all-silica $C_{5\text{-ring}}$.

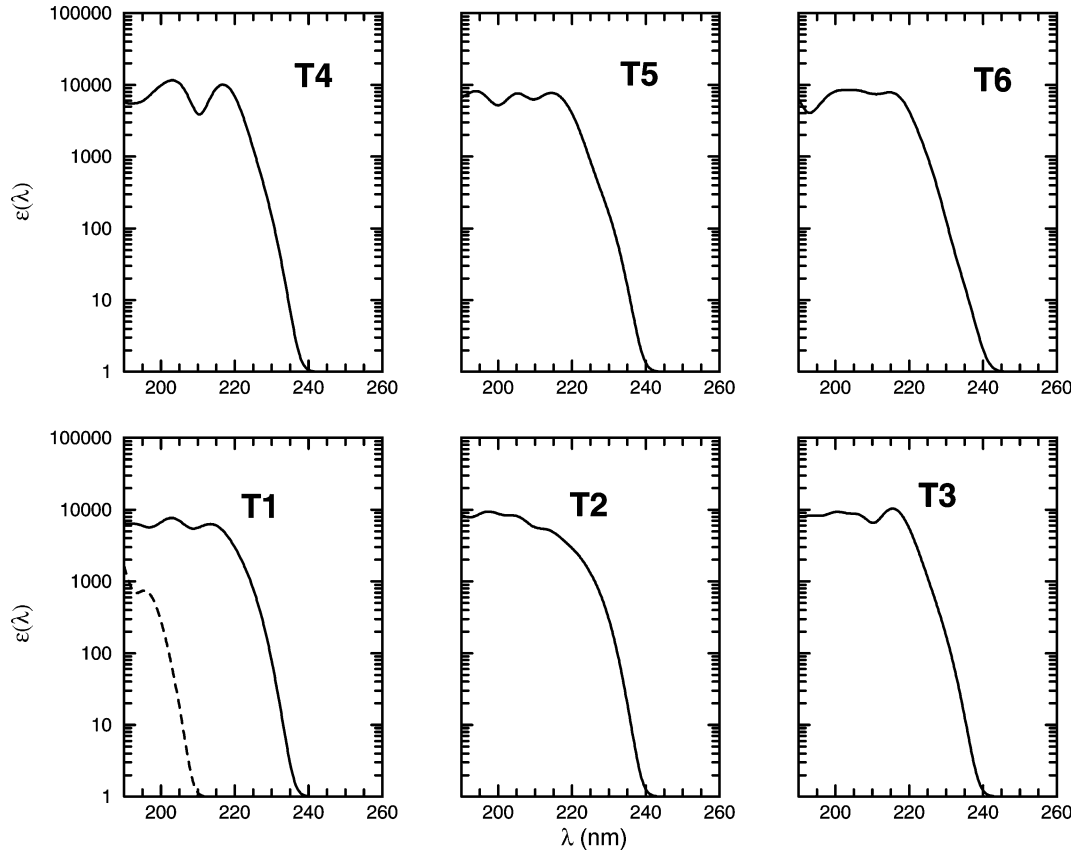

Figure 5. Calculated TD-DFT excitation spectra of cluster models cut from $[Ti_1Si_{95}O_{192}]$ DFT-optimized structures. Calculated spectra are relative to C_{tetra}, with Ti in the T1, T2, T3, T4, T5, and T6 sites. The excitation spectrum for a C_{tetra} all-silica cluster (site T1) is reported for comparison (dashed line).

(T10) to 0.95 eV (T8), and the LUMO − LUMO + 1 separation ($e_g^{(E)}$ splitting) varies between 0.045 (T4) and 0.174 eV (T6).

As a first approximation, a CFT-like description could also be adopted for the 32 higher-energy occupied states of the C_{tetra}

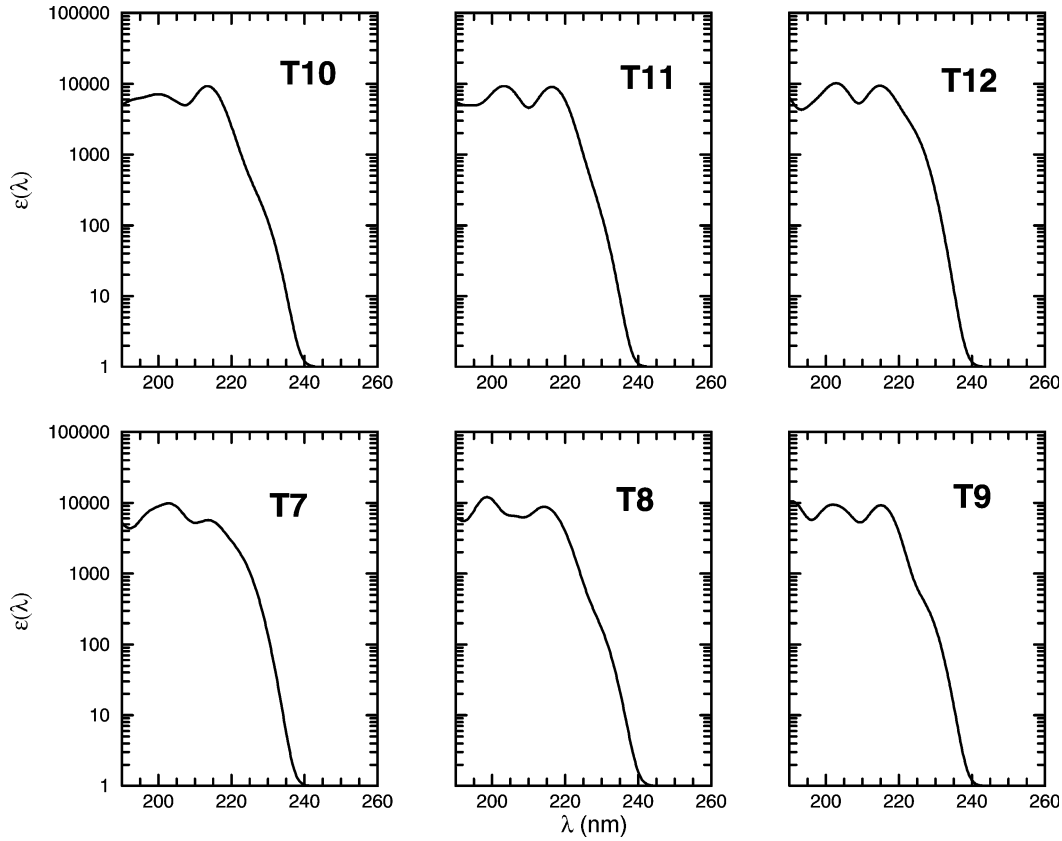

Figure 6. Calculated TD-DFT excitation spectra of cluster models cut from $[Ti_1Si_{95}O_{192}]$ DFT-optimized structures. Calculated spectra are relative to C_{tetra} with Ti in the T7, T8, T9, T10, T11, and T12 sites.

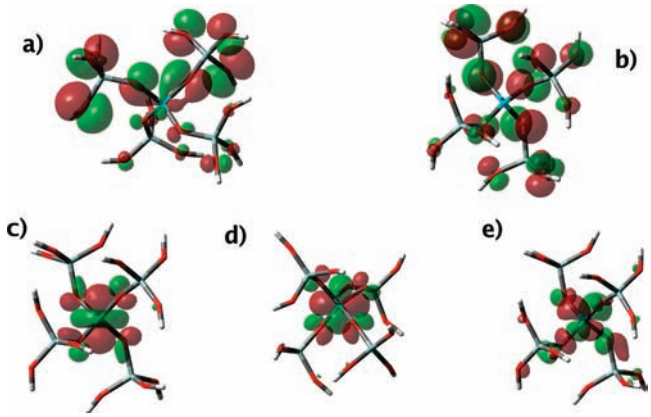

Figure 7. Representative examples of frontier molecular orbitals involved in electronic transitions in one C_{tetra} (Ti−(O−Si(OH)$_3$)$_4$) cluster, Ti in T6. (a) b-$t_{2g}^{(O)}$ occupied orbital; (b) nb-$t_{2g}^{(O)}$ occupied orbital; (c) $e_g^{(E)}$ unoccupied orbital; (d) $e_g^{(E)}$ unoccupied orbital; (e)$t_{2g}^{(E)}$ unoccupied orbital. Green and red contours represent positive and negative orbital lobes, respectively. Atom color codes: Ti, cyan; Si, gray; O, red; H, white.

models, where the dominant contribution comes from the O 2p lone pairs (two for each of the 16 O atoms). In tetrahedral symmetry, they are split into three groups that could be labeled $t_{2g}^{(O)}$, $t_{2g}^{(O-1)}$, and $e_g^{(O)}$ in decreasing energy order (with O indicating "occupied"). These MOs contain, however, nonnegligible contributions of the Ti d orbitals. Thus, in addition to the details of T-site geometry and symmetry, their energy ladder also depends on the extent of contamination with metal states. Actually, the details of the electronic structure in the frontier MOs region change among the 12 T site models, and such variations are not straightforwardly related to simple structural parameters, such as Ti−O bond distances. These observations explain why the calculated spectra differ in the number, position, and intensity of the peaks and, at the same time, suggest that determining Ti siting simply from analysis of UV−vis band profiles could be a very difficult task, even in the case of a nondefective TS-1. Indeed, optical spectra of systems characterized by different Ti locations share a number of common features, as detailed below.

A graphical representation of relevant orbitals is shown in Figure 7 for the case of Ti in T6. The occupied MOs involved in electronic transitions are the $t_{2g}^{(O)}$'s. In the C_{tetra} clusters, they correspond to the 12 states from HOMO to HOMO − 11 and may be grouped into two subsets. Although the higher energy $t_{2g}^{(O)}$ states are basically nonbonding O 2p combinations (nb-$t_{2g}^{(O)}$), the ones at lower energy are characterized by mixing with Ti d states and therefore present a certain degree of Ti−O bonding character (b-$t_{2g}^{(O)}$). Moreover, the frontier-occupied MOs are not strictly localized on the Ti-bound oxygens, but should formally be regarded as extended over all the oxygens in the model system. Such an electronic structure description holds for larger $C_{5\text{-ring}}$ models, as well, as clearly shown in Figure 8. In particular, although the HOMO is localized mainly on the Ti-bound oxygens, other nb-$t_{2g}^{(O)}$'s are delocalized over the whole 5-ring system. Therefore, by extrapolating to the solid, LMCT electronic transitions in low-Ti-content TS-1 essentially go from the $t_{2g}^{(O)}$ band to the localized Ti d states.

The edge (lowest energy absorption) of the calculated spectra, ranging from 223.2 (T1) to 230.7 (T6) nm, is mainly due to the HOMO → LUMO transition, with significant contributions from the HOMO − 1 → LUMO and HOMO − 2 → LUMO excitations. The higher wavelength peak (210−225 nm) is due to nb-$t_{2g}^{(O)}$ → $e_g^{(E)}$ transitions and has a pure LMCT character, whereas bands between 195 and 210 nm derive from b-$t_{2g}^{(O)}$ →

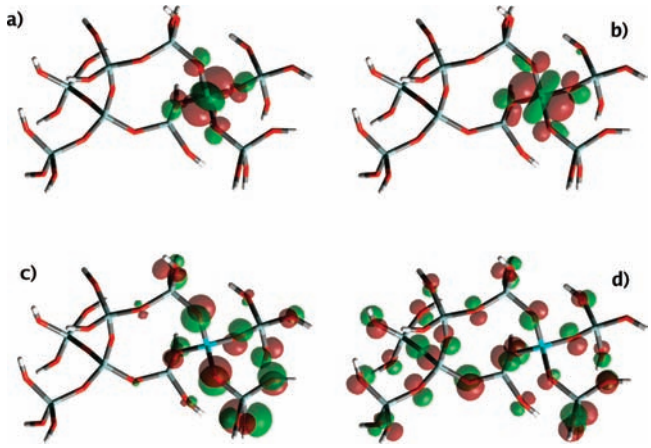

Figure 8. Representative examples of frontier molecular orbitals involved in electronic transitions for a $C_{5\text{-ring}}$ structure with one Ti (in T6). (a) $e_g^{(E)}$ unoccupied orbital; (b) $e_g^{(E)}$ unoccupied orbital. (c) nb-$t_{2g}^{(O)}$ occupied orbital (HOMO); (d) nb-$t_{2g}^{(O)}$ occupied orbital. Color codes as in Figure 7.

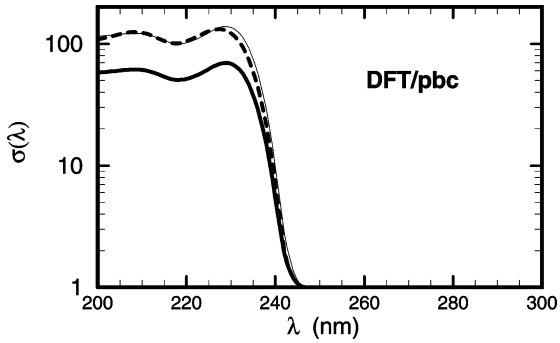

Figure 9. DFT optical conductivity σ calculated for crystal structures (with pbc). Wide, solid line: $[Ti_1Si_{95}O_{192}]$ structure with one Ti in T3. Dashed line: $[Ti_2Si_{94}O_{192}]$ structure with Ti in two well-separated T3 sites (Ti−Ti distance = 14.0 Å). Narrow, solid line: twice the optical conductivity σ calculated for the $[Ti_1Si_{95}O_{192}]$ structure with one Ti in T3.

$e_g^{(E)}$ transitions and might be considered LMCT contaminated by O 2p−Ti d mixing. Interestingly, the $t_{2g}^{(E)}$ states do not contribute to the bands above 200 nm because of their quite large energy separation from the $e_g^{(E)}$'s. Indeed, absorptions below 190 nm are mainly related to lower-intensity $t_{2g}^{(O)} \rightarrow t_{2g}^{(E)}$ transitions; however, in the real material, such bands should be at least partially obscured by the silica matrix absorptions.

Let us now consider the excitation spectra for the higher-Ti-content TS-1 systems (Figures 9−11). It should be stressed at the outset that, also in this case, DFT/pbc and TDDFT/cluster approaches provide very close representations of electronic excitation properties, leading to similar band profiles and peak position differences in the 10 nm range (Figures 10, 11).

Electronic spectra were calculated for models characterized by different arrangements of the two Ti atoms in the TS-1 cell. In particular, T site locations and Ti^1-Ti^2 separations were selected with the aim of discriminating in the calculated spectra the effect of the Ti content increase (Figure 9) from that of the Ti−Ti interaction (Figures 10 and 11).

The effect of Ti content on TS-1 electronic spectra is cleary pictured in Figure 9. Here, a $[Ti_2Si_{94}O_{192}]$ model with two Ti atoms located in two T3 sites separated by 14 Å has been considered, and electronic excitations have been calculated with the DFT/pbc approach. Remarkably, the optical conductivity of this system amounts to twice that calculated for $[TiSi_{95}O_{192}]$

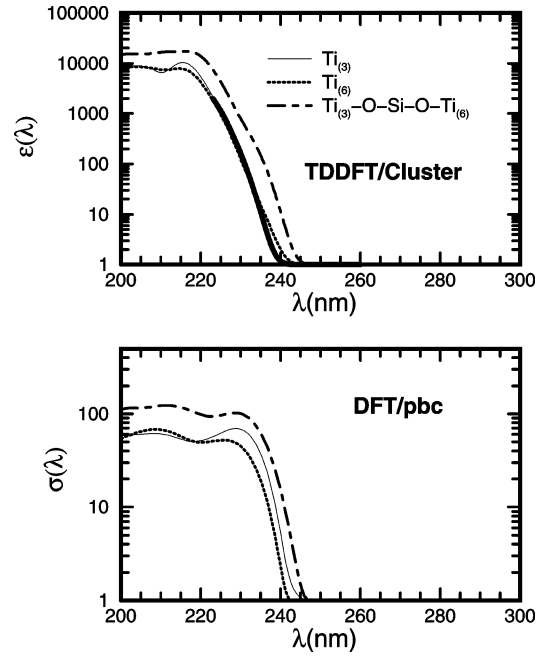

Figure 10. Top: TD-DFT absorbance spectra calculated for cluster models. Narrow, solid line: C_{tetra} cluster with Ti in T3. Wide, dotted line, C_{tetra} cluster with Ti in T6. Wide dotted, dashed line: $C_{5\text{-ring}}$ with a Ti−O−Si−O−Ti bridge (Ti in T3 and T6) cut from $[Ti_2Si_{94}O_{192}]$. Bottom: DFT optical conductivity σ calculated for crystal structures (with pbc). Narrow, solid line: $[TiSi_{95}O_{192}]$ with Ti in T3. Wide, dashed line: $[TiSi_{95}O_{192}]$ with Ti in T6. Wide, dotted, dashed line: $[Ti_2Si_{94}O_{192}]$ system with Ti^1 in T3 and Ti^2 in T6.

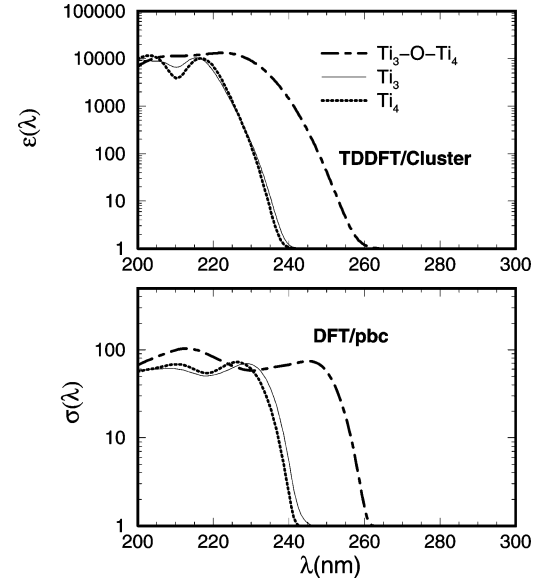

Figure 11. Top: TD-DFT absorbance spectra calculated for cluster models cut from $[Ti_1Si_{95}O_{192}]$ with Ti in T3 (narrow line) and T4 (wide dotted line) and from a $[Ti_2Si_{94}O_{192}]$ (with Ti in T3 and T4) corresponding to a Ti−O−Ti structure. Bottom: DFT optical conductivity calculated for the crystal structures (with pbc). Narrow, black line: one Ti in T3. Wide, dashed line: one Ti in T4. Wide, dotted, dashed line: double Ti substitution in both T3 and T4.

with Ti in T3. On this basis, it could be predicted that UV−vis spectra of TS-1 systems with well-separated (noninteracting) Ti centers will be characterized by an intensity proportional to the Ti content; that is, following the Beer−Lambert law. Closer Ti centers should lead to deviations from the Beer−Lambert behavior. Such a prediction is confirmed by comparing electronic spectra of systems containing two close Ti atoms with

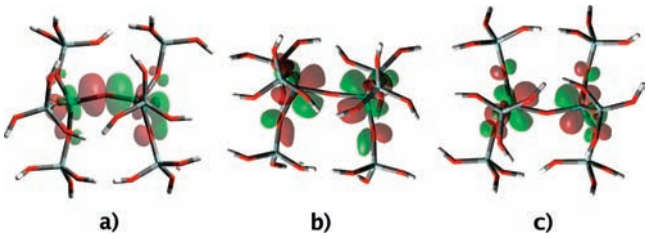

Figure 12. Relevant molecular orbitals in a cluster model containing a Ti−O−Ti bridge. (a) Bonding MO with dominant d_{z^2} character; (b) LUMO, formed by combination of Ti d states from both Ti centers; (c) LUMO + 1, formed by combination of Ti d states from both Ti centers. Color codes as in Figure 7.

those of the corresponding low-Ti-content models. In the case of a representative Ti−O−Si−O−Ti structure, for which Ti^1 is in T3, Ti^2 is in T6, and the Ti^1-Ti^2 separation amounts to 5.605 Å, Beer−Lambert-like behavior is still observed: intensities are approximately additive, and only a small red shift of the edge is detected (see Figure 10). Indeed, analysis of the TD-DFT excitations and the MOs involved in the transitions indicates that the presence of two nonadjacent Ti centers perturbs but does not substantially alter the electronic structure of the TS-1 system with respect to the case of "isolated" (or well-separated) Ti centers. Therefore, the optical spectrum of a system with two TiO_4 units interconnected by a Si in close T sites could approximately be described as the sum of two spectra, each related to isolated TiO_4 in one of the sites (namely, T3 and T6). In the present case, the absorption edge corresponds to the lowest energy transition in the T6 system, whereas the excitation responsible of the spectral edge of the T3 system could be identified at 224.6 nm. Indeed, the orbitals involved in the UV−vis transitions resemble the frontier orbitals of the C_{tetra} clusters with Ti in T3 and T6. For instance, the HOMO is mainly localized on the 2p oxygens around Ti in T6, whereas the HOMO − 1 is spread over all oxygens of the 5-ring. All of the lowest unoccupied MOs have Ti 3d character: In particular, the LUMO and LUMO + 1 are mainly related to Ti d states in T6 with a minor contribution of Ti-d in T3, whereas LUMO + 2 is predominantly localized on T3 and slightly contaminated by Ti-d in T6. Therefore, a small degree of mixing between Ti d states is present, thus allowing partial delocalization of the lowest unoccupied MOs on nearest-neighboring Ti centers.

On the other hand, direct interaction between Ti centers such as in the Ti−O−Ti bridge ($Ti^1-Ti^2 = 3.495$ Å, with Ti^1 in T3 and Ti^2 in T4) leads to a large red shift of the UV−vis edge (to 248 nm) as well as to significant modifications in the absorption profiles (Figure 11). Such a pronounced change arises from drastic alterations in the TS-1 electronic structure. In particular, the lowest unoccupied states could no longer be described as Ti d states in a tetrahedral CFT because the TiO_4 units forming the Ti−O−Ti moiety do share an oxygen atom and are, therefore, bonded to each other. This allows d-orbital mixing between Ti centers, with relevant consequences on both electronic excitation and bonding properties. Concerning the latter, electronic structure analysis highlighted that several low-energy MOs (not involved in optical transitions) delocalized on the Ti−O−Ti moiety contain a major contribution of Ti d states and are characterized by a pronounced bonding character in the Ti−O−Ti region (Figure 12). Such a large Ti-d participation in bonding is responsible for a particularly strong Ti−O−Ti interaction and explains why the Ti−O bond distances in the bridge are the shortest ones (see Table 3). However, not only does d−d mixing stabilize the bonding states but also its effect is even greater on the lowest unoccupied MOs, the LUMO and LUMO + 1, which correspond to the arrival states of the lowest-energy electronic transitions: as a result, the edge of the excitation spectrum is red-shifted.

Actually, from detailed assignment of the spectral bands, it emerges that all absorptions beyond 205 nm involve excitations to the LUMO and LUMO + 1 orbitals. The absorption edge is due to the HOMO → LUMO transition, with the HOMO showing a pure nonbonding O 2p character, such as in the case of low-Ti-content systems. However, the maximum peak (at 225 nm) is due to excitations starting from b-$t_{2g}^{(O)}$-like states in which the extent of Ti-d contamination is higher than in the isolated Ti center cases. Also at smaller wavelengths, the bands could be generally ascribed to excitations from delocalized O 2p states with smaller Ti d character to low-energy empty states deriving from the combination of the empty d orbitals. Interestingly, such excited states (Figure 12b, c) are spread over the Ti−O−Ti moiety and evenly localized on both Ti centers. Therefore, d−d mixing also causes excited electrons to be more delocalized with respect to the case of an isolated Ti center.

4. Summary and conclusions

Nondefective TS-1 models have been investigated by means of periodic DFT calculations with the aim of contributing to the issue of Ti preferential positioning. The molecular complexity underlying the TS-1 synthesis process makes it difficult to single out the factor that actually determines Ti preferential location in such a relevant material.[19] Nevertheless, from the results here presented, a nonrandom Ti siting in TS-1 emerged on the basis of thermodynamics (energetics) considerations only.

For a Ti content corresponding to 1.35% in weight of TiO_2 (one Ti in 96 T sites), the structures with titanium siting in T3 or T4 are the most probable.

The siting problem becomes more involved for higher Ti content, here analyzed in a limited set of possible structures corresponding to a Ti content of 2.70% in weight of TiO_2 (i.e., 2 Ti over 96 T sites). In this case, both the kind of Ti sites and their Ti−Ti separation play a relevant role for the relative stability.

Quite interestingly, the presence of a Ti−O−Ti bridge (Ti−Ti distance of 3.5 Å), in which both Ti's are in a tetrahedral TiO_4 geometry, is not particularly destabilized with respect to different double-Ti substitutions. Actually, one such structure is only 2.7 kcal/mol higher in energy with respect to the most stable one in the sampled configurations.

Starting from the optimized periodic structures, electronic excitation spectra were obtained by adopting a cluster approach and a TD-DFT calculation scheme. All of the different Ti sites present absorption profiles in the 200−230 nm UV region, in line with DRUV−vis experiments on low Ti content dry TS-1 samples. The excitations present a multiband profile that is characteristic of each different T site. The actual profiles are strictly interlaced with distortion from the perfect tetrahedral symmetry, which is different for different crystallographic sites. The absorption bands involve transitions from oxygen lone pairs to empty d states localized on Ti (i.e., LMCT: ligand-to-metal charge transfer transitions), in line with the current opinion.

Our results, however, suggest a description more complex than the standard picture, based on $O^{2-} + Ti^{4+} \rightarrow O^- + Ti^{3+}$ transitions involving only Ti-bound oxygen atoms. Actually, we propose that UV−vis transitions in titanium zeolites would occur from framework oxygen bands to localized Ti empty states. The participation of extended electronic structures to the UV transitions in Ti zeolites may be a key point in explaining

the photoconducting properties recently highlighted in Ti zeolites (TS-1 included).[3]

In addition to electronic excitations, analysis of the vibrational properties has been performed. From the investigations on isolated Ti sites, a picture in line with previous analysis emerges: the 960 cm^{-1} band in the IR transparent silica window can be associated with tetrahedral Ti, along with a Raman-active feature detected at 1125 cm^{-1}. Some interesting features, however, emerged from the vibrational spectra of Ti−O−Si−O−Ti and Ti−O−Ti bridges. Associated with the first structure, we have found an IR-active band just in the center of the silica window, at 908 cm^{-1}, that could be easily detectable in the experimental IR spectra. The absence of such a band in the available IR spectra of TS-1 indicates that the presence of such a structure can be excluded in real TS-1. More problematic could be the clear-cut exclusion of a Ti−O−Ti bridge: indeed, this structure gives IR signatures (853 and 1003 cm^{-1}) that are just at the edge of the silica window. In addition, an intense Raman-active mode calculated at 1115 cm^{-1} can be compatible with the tetrahedral Ti "Raman signature" at 1125 cm^{-1}. Moreover, its calculated absorption edge at 248 nm is compatible with available TS-1 data. Probably such a (tetrahedral Ti) Ti−O−Ti structure could be considered a nucleation center for the (octahedral Ti) TiO_2 phase separation. Indeed, for the TiO_2 phase growth, which is known to occur at Ti contents higher than 2.5%, Ti−O−Ti bridges should be formed. Our results, which demonstrate the stability of this moiety in models of comparable Ti content, its compatibility with available spectroscopic data, and its peculiar electronic properties, suggest therefore further experimental work aimed at the identification and characterization of Ti−O−Ti bridges in the TS-1 framework.

References and Notes

(1) Clerici, M. G.; Bellussi, G.; Romano, U. *J. Catal.* **1991**, *129*, 159.

(2) Taramasso, M.; Perego, G.; Notari, B. U.S. Patent 441051, 1983.

(3) Atienzar, P.; Valencia, S.; Corma, A.; Garcia, H. *ChemPhysChem* **2007**, *8*, 1115.

(4) Baerlocher, C.; Meier, W. M.; Olson, D. H. *Atlas of Zeolite Framework Types*; Elsevier: The Netherlands, 2001.

(5) van Köningsveld, H.; van Bekkum, H.; Jansen, J. C. *Acta Crystallogr., B* **1987**, *43*, 127.

(6) Millini, R.; Perego, G.; Berti, D.; Parker, W. O.; Carati, A.; Bellussi, G. *Microporous Mesoporous Mater.* **2000**, *35*−*36*, 387.

(7) Millini, R.; Previdi Massara, E.; Perego, G.; Bellussi, G. *J. Catal.* **1992**, *137*, 497.

(8) Scarano, D.; Zecchina, A.; Bordiga, S.; Geobaldo, F.; Spoto, G.; Petrini, G.; Leofanti, G.; Padovan, M.; Tozzola, G. *J. Chem. Soc. Faraday Trans.* **1993**, *89*, 4123.

(9) Li, C.; Xiong, G.; Xin, Q.; Liu, J.; Ying, P.; Feng, Z.; Li, J.; Yang, W.; Wang, Y.; Wang, G.; Liu, X.; Lin, M.; Wang, X.; Min, E. *Angew. Chem., Int. Ed.* **1999**, *38*, 2320.

(10) Le Noc, L.; Trong On, D.; Solomykina, S.; Echchahed, B.; Beland, F.; Cartier Dit Moulin, C.; Bonneviot, L. *Stud. Surf. Sci. Catal.* **1996**, *101*, 611.

(11) Lamberti, C.; Bordiga, S.; Arduino, D.; Zecchina, A.; Geobaldo, F.; Spanó, G.; Genoni, F.; Petrini, G.; Carati, A.; Villain, F.; Vlaic, G. *J. Phys. Chem. B* **1998**, *102*, 6382.

(12) Lamberti, C.; Bordiga, S.; Zecchina, A.; Artioli, G.; Marra, G.; Spanó, G. *J. Am. Chem. Soc.* **2001**, *123*, 2204.

(13) Hijar, C. A.; Jacubinas, R. M.; Eckert, J.; Henson, N. J.; Hay, P. J.; Ott, K. C. *J. Phys. Chem. B* **2000**, *104*, 12157.

(14) Henry, P. F.; Weller, M. T.; Wilson, C. C. *J. Phys. Chem. B* **2001**, *105*, 7452.

(15) Deka, R. C.; Nasluzov, V. A.; Ivanova Shor, E. A.; Shor, A. M.; Vayssilov, G. N.; Rösch, N. *J. Phys. Chem. B* **2005**, *109*, 24304.

(16) Ricchiardi, G.; de Man, A. J. M.; Sauer, J. *Phys. Chem. Chem. Phys.* **2000**, *2*, 2195.

(17) Sastre, G.; Corma, A. *Chem. Phys. Lett.* **1999**, *302*, 447.

(18) Millini, R.; Perego, G.; Seiti, K. *Stud. Surf. Sci. Catal.* **1994**, *84*, 2123.

(19) Parker, W. O.; Millini, R. *J. Am. Chem. Soc.* **2006**, *128*, 1450.

(20) Boccuti, M. R.; Rao, K. M.; Zecchina, A.; Leofanti, A.; Petrini, G. *Stud. Surf. Sci. Catal.* **1988**, *48*, 133.

(21) Perdew, J. P.; Burke, K.; Ernzerhof, M. *Phys. Rev. Lett.* **1996**, *77*, 3865–3868.

(22) Vanderbilt, D. *Phys. Rev. B* **1990**, *41*, 7892.

(23) He, Y.; Tilocca, A.; Dulub, O.; Selloni, A.; Diebold, U. *Nat. Mat.* **2009**, *8*, 585.

(24) Tilocca, A.; Fois, E. *J. Phys. Chem. C* **2009**, *113*, 8683.

(25) Trudu, F.; Tabacchi, G.; Gamba, A.; Fois, E. *J. Phys. Chem. A* **2007**, *111*, 11626.

(26) Trudu, F.; Tabacchi, G.; Gamba, A.; Fois, E. *J. Phys. Chem. C* **2008**, *112*, 15394.

(27) CPMD code (www.cpmd.org): Copyright MPI für Festkörperforschung, Stuttgart, and IBM Zürich Research Laboratory, 1990−2006.

(28) Runge, E.; Gross, E. K. *Phys. Rev. Lett.* **1984**, *52*, 997.

(29) Casida, M. E.; Jamorsky, C.; Casida, K. C.; Salahub, D. R. *J. Chem. Phys.* **1998**, *108*, 4439.

(30) Becke, A. D. *J. Chem. Phys.* **1993**, *98*, 5648.

(31) Frisch, M. J.; Trucks, G. W.; Schlegel, H. B.; Scuseria, G. E.; Robb, M. A.; Cheeseman, J. R.; Montgomery, J. A., Jr.; Vreven, T.; Kudin, K. N.; Burant, J. C.; Millam, J. M.; Iyengar, S. S.; Tomasi, J.; Barone, V.; Mennucci, B.; Cossi, M.; Scalmani, G.; Rega, N.; Petersson, G. A.; Nakatsuji, H.; Hada, M.; Ehara, M.; Toyota, K.; Fukuda, R.; Hasegawa, J.; Ishida, M.; Nakajima, T.; Honda, Y.; Kitao, O.; Nakai, H.; Klene, M.; Li, X.; Knox, J. E.; Hratchian, H. P.; Cross, J. B.; Bakken, V.; Adamo, C.; Jaramillo, J.; Gomperts, R.; Stratmann, R. E.; Yazyev, O.; Austin, A. J.; Cammi, R.; Pomelli, C.; Ochterski, J. W.; Ayala, P. Y.; Morokuma, K.; Voth, G. A.; Salvador, P.; Dannenberg, J. J.; Zakrzewski, V. G.; Dapprich, S.; Daniels, A. D.; Strain, M. C.; Farkas, O.; Malick, D. K.; Rabuck, A. D.; Raghavachari, K.; Foresman, J. B.; Ortiz, J. V.; Cui, Q.; Baboul, A. G.; Clifford, S.; Cioslowski, J.; Stefanov, B. B.; Liu, G.; Liashenko, A.; Piskorz, P.; Komaromi, I.; Martin, R. L.; Fox, D. J.; Keith, T.; Al-Laham, M. A.; Peng, C. Y.; Nanayakkara, A.; Challacombe, M.; Gill, P. M. W.; Johnson, B.; Chen, W.; Wong, M. W.; Gonzalez, C.; Pople, J. A. *Gaussian 03, Revision D.02*; Gaussian, Inc.: Wallingford, CT, 2004.

(32) Kleinman, L.; Bylander, D. M. *Phys. Rev. Lett.* **1982**, *48*, 1425.

(33) Troullier, N.; Martins, J. L. *Phys. Rev. B* **1991**, *43*, 1993.

(34) Spanó, E.; Tabacchi, G.; Gamba, A.; Fois, E. *J. Phys. Chem. B* **2006**, *110*, 21651–21661.

(35) Fois, E.; Gamba, A.; Tabacchi, G. *ChemPhysChem* **2005**, *6*, 1237.

(36) Fois, E.; Gamba, A.; Tabacchi, G. *ChemPhysChem* **2008**, *9*, 538.

(37) Scott, A. P.; Radom, L. *J. Phys. Chem.* **1996**, *100*, 16502.

(38) Ricchiardi, G.; Damin, A.; Bordiga, S.; Lamberti, C.; Spanó, G.; Rivetti, F.; Zecchina, A. *J. Am. Chem. Soc.* **2001**, *123*, 11409.

(39) Bordiga, S.; Coluccia, S.; Lamberti, C.; Marchese, L.; Zecchina, A.; Boscherini, F.; Buffa, F.; Genoni, F.; Leofanti, G.; Petrini, G.; Vlaic, G. *J. Phys. Chem.* **1994**, *98*, 4125.

(40) Fan, W.; Duan, R.-G.; Yokoi, T.; Wu, P.; Kubota, Y.; Tatsumi, T. *J. Am. Chem. Soc.* **2008**, *130*, 10150.

JP905110S